

Magnetically driven superconductivity in CeCu_2Si_2

O. Stockert,^{1,*} J. Arndt,¹ E. Faulhaber,^{2,3} C. Geibel,¹ H. S. Jeevan,^{1,4} S. Kirchner,^{1,5}

M. Loewenhaupt,² K. Schmalzl,⁶ W. Schmidt,⁶ Q. Si,⁷ and F. Steglich¹

¹*Max-Planck-Institut für Chemische Physik fester Stoffe, 01187 Dresden, Germany*

²*Institut für Festkörperphysik, Technische Universität Dresden, 01062 Dresden, Germany*

³*Gemeinsame Forschergruppe Helmholtz-Zentrum*

Berlin - TU Dresden, 85747 Garching, Germany

⁴*I. Physikalisches Institut, Universität Göttingen, 37077 Göttingen, Germany*

⁵*Max-Planck-Institut für Physik komplexer Systeme, 01187 Dresden, Germany*

⁶*Jülich Centre for Neutron Science at Institut Laue-Langevin, 38042 Grenoble, France*

⁷*Department of Physics and Astronomy,*

Rice University, Houston, Texas, 77005, USA

(Dated: October 31, 2018)

Abstract

PACS numbers:

*Electronic address: stockert@cpfs.mpg.de

The origin of unconventional superconductivity, including high-temperature and heavy-fermion superconductivity, is still a matter of controversy. Spin excitations instead of phonons are thought to be responsible for the formation of Cooper pairs. Using inelastic neutron scattering, we present the first in-depth study of the magnetic excitation spectrum in momentum and energy space in the superconducting and the normal states of CeCu_2Si_2 . A clear spin excitation gap is observed in the superconducting state. We determine a lowering of the magnetic exchange energy in the superconducting state, in an amount considerably larger than the superconducting condensation energy. Our findings identify the antiferromagnetic excitations as the major driving force for superconducting pairing in this prototypical heavy-fermion compound located near an antiferromagnetic quantum critical point.

While conventional superconductivity (SC) is generally incompatible with magnetism, magnetic excitations seem to play an important role in the Cooper pair formation of unconventional superconductors such as the high- T_c cuprates or the low- T_c organic and heavy-fermion (HF) superconductors. Since the discovery of SC in CeCu_2Si_2 ¹, antiferromagnetic (AF) spin excitations have been proposed as a viable mechanism for SC²⁻⁴. The discovery of SC at the boundary of AF order in CePd_2Si_2 ⁵ has pushed this notion into the framework of AF quantum criticality⁶. Unfortunately, such quantum critical points (QCPs) proximate to HF superconductors typically arise under pressure, which makes it difficult to probe their magnetic excitation spectrum.

Here, we report a detailed study of the magnetic excitations in CeCu_2Si_2 , which exhibits SC below $T_c \approx 0.6\text{ K}$. This prototypical HF compound is ideally suited for our purpose, since SC here is in proximity to an AF QCP already at ambient pressure (cf. Fig. 1(a)). As displayed in Fig. 1(b) CeCu_2Si_2 crystallises in a structure with body-centred tetragonal symmetry and is one of the best studied HF superconductors and well characterised by low-temperature transport and thermodynamic measurements⁷. Moreover, those measurements in the field-induced normal state have already provided evidence that the QCP in this compound is of the three-dimensional (3D) spin-density-wave (SDW) type⁸. The spatial anisotropy of the spin fluctuations in superconducting CeCu_2Si_2 was measured at $T = 0.06\text{ K}$ and at an energy transfer $\hbar\omega = 0.2\text{ meV}$ and is shown in Fig. 1(c). These magnetic correlations display only a small anisotropy (a factor of 1.5) in the correlation lengths

between the [110] and the [001] direction. Therefore, these quite isotropic spin fluctuations are in line with thermodynamic and transport measurements exhibiting $C/T = \gamma_0 - a\sqrt{T}$ or $\rho - \rho_0 = AT^\alpha$, $\alpha = 1 - 1.5^{8,9}$, and strongly support a three-dimensional quantum critical SDW scenario¹⁰. We are able to identify the magnetic excitations in the normal state of paramagnetic, superconducting CeCu₂Si₂, around the incommensurate wave vector⁹ of the SDW order nearby in the phase diagram (cf. Fig. 1(a)), and further establish the system's proximity to the AF QCP through the observation of a considerable slowing down in the spin dynamics. Going into the superconducting state, a spin gap opens out of a broadened quasielastic response which extends to much higher frequencies ($10 \times$ the superconducting gap). These data allow us to establish a saving in the AF exchange energy that is considerably larger than the superconducting condensation energy, thereby providing the first demonstration of the nearly-quantum-critical AF excitations as the major driving force for unconventional SC.

Superconductivity and antiferromagnetism in CeCu₂Si₂

The SC in CeCu₂Si₂ we consider is close to the AF QCP, and is to be contrasted with a second superconducting dome appearing at high pressure which is thought to be associated with a valence instability and the concomitant fluctuations^{9,12}. This AF QCP is located within the narrow homogeneity range of the "122" phase in the ternary chemical Ce-Cu-Si phase diagram of this tetragonal compound². Correspondingly, we can prepare *homogeneous* samples (with slight Cu deficit) from the antiferromagnetically ordered side (A-type) and (with tiny Cu excess) from the paramagnetic, superconducting side of the QCP (S-type); by contrast, crystals very close to the 1 : 2 : 2 stoichiometry exhibit a ground state where SC and AF compete with each other without microscopic coexistence (A/S-type)². The AF order was found to be an incommensurate SDW⁹. At $T = 0.05$ K, well below $T_N \approx 0.8$ K, the A-type CeCu₂Si₂ exhibits an ordered magnetic moment $\mu_{ord} \approx 0.1 \mu_B$ and an incommensurate propagation vector $\tau \approx (0.215 \ 0.215 \ 0.53)$. The latter can be ascribed to a nesting wave vector of the renormalised Fermi surface. However, a full microscopic description of the magnetic order remains to be addressed.

In order to study the superconducting state in CeCu₂Si₂ in detail, neutron scattering results¹⁴ on an S-type single crystal are presented in this Article. A previous experiment

was severely hampered by a large experimental background and a low signal-to-background ratio¹⁵. Thermodynamic measurements confirmed that this crystal is superconducting with a $T_c \approx 0.6$ K and an upper critical field $B_{c2}(T = 0) < 2$ T¹⁴. Elastic neutron scattering measurements did not feature resolution-limited magnetic Bragg peaks in S-type CeCu₂Si₂ in accordance with thermodynamic measurements. However, at positions where magnetic satellite peaks are observed in A-type CeCu₂Si₂⁹, e.g., at $\mathbf{Q}_{\text{AF}} = (0.215 \ 0.215 \ 1.458)$, relative to a nearby nuclear Bragg reflection \mathbf{G} ($\mathbf{Q}_{\text{AF}} = \mathbf{G} \pm \tau$), the S-type crystal exhibits quite weak correlation peaks at low temperatures¹⁵. They are still present above T_c and disappear at $T \approx 0.8$ K, very similar to the behaviour of the SDW order in A-type CeCu₂Si₂⁹. Although these peaks were found to be purely elastic within the energy resolution (≈ 57 μ eV), their linewidth in \mathbf{Q} space is considerably broadened corresponding to a correlation length of 50 – 60 Å being comparable to the superconducting coherence length of order 100 Å⁴. Thus, static magnetically ordered regions seem to exist in a quite small part of the sample and are separated from the surrounding superconducting regions.

Spin dynamics in CeCu₂Si₂

We probe the magnetic response of CeCu₂Si₂ through extensive inelastic neutron scattering measurements around $\mathbf{Q} = \mathbf{Q}_{\text{AF}} = (0.215 \ 0.215 \ 1.458)$, since no appreciable magnetic intensity has been detected elsewhere in the Brillouin zone. Fig. 2(a) displays energy scans at this \mathbf{Q}_{AF} position and at a general position $\mathbf{Q} = \mathbf{Q}_{\text{arb}} = (0.1 \ 0.1 \ 1.6)$, where no correlation peaks emerge, but which has the same $|\mathbf{Q}|$. Both data sets were recorded in the superconducting state at $T = 0.07$ K. At \mathbf{Q}_{arb} only the incoherent elastic background contribution with instrument resolution is seen, while no magnetic intensity could be detected. In contrast, at \mathbf{Q}_{AF} the response shows a strong inelastic signal with a long tail of the intensity extending beyond $\hbar\omega = 2$ meV (cf. inset of Fig. 2(a)). The missing spectral weight at low energies is an indication for a spin-excitation gap in the superconducting state. The spectrum recovers the missing weight at the gap edge, thereby constituting an inelastic line. The data can be described by a quasielastic Lorentzian line with a spin excitation gap $\hbar\omega_{\text{gap}} \approx 0.2$ meV and with a density of states as for the electronic gap of a d-wave BCS superconductor (solid lines in Figs. 2(a) and 3(a)). $\hbar\omega_{\text{gap}} \approx 3.9k_B T_c$ is found to be 10% smaller than the value predicted for a weak-coupling d-wave superconductor¹⁷ and falls 20%

below $2\Delta_0/k_B T_c = 5.0$ as determined by Cu-NQR for CeCu_2Si_2 ^{18,19}. To unambiguously relate the inelastic magnetic excitation to the superconducting state, it was necessary to perform additional measurements in the normal state.

Energy scans recorded at \mathbf{Q}_{AF} in the normal state are shown in Fig. 2(b). Notably, independent of how the normal state is reached, i.e., above T_c at $T = 0.8\text{ K}$ and $B = 0$ or above B_{c2} at $T = 0.07\text{ K}$ and $B = 2\text{ T}$, the magnetic response is almost identical and appears to be quasielastic. The fits to the quasielastic magnetic response with a Lorentzian lineshape give a good description of the data as seen in Figs. 2(b) and 3(a). With increasing temperature in the normal state the magnetic response weakens in intensity and broadens considerably. Starting from $\Gamma \approx 0.11\text{ meV}$ at $T = 0.07\text{ K}$ the linewidth of the quasielastic response at \mathbf{Q}_{AF} increases to $\Gamma \approx 0.235\text{ meV}$ at $T = 1.7\text{ K}$ (Fig. 3(b)). This considerable slowing down of the response when lowering the temperature indicates the proximity of S-type CeCu_2Si_2 to the AF QCP. $\Gamma(T)$ extrapolates to a finite value at $T \rightarrow 0$, since the S-type single crystal is located on the paramagnetic side of the QCP (cf. Fig. 1(a)). A related critical slowing down was observed in magnetically ordered A-type CeCu_2Si_2 ²⁰.

The fact that the magnetic excitation gap disappears in the normal state, i.e., above T_c , and also above B_{c2} at low temperatures, where the magnetic short-range correlations still persist, gives direct evidence that the spin gap $\hbar\omega_{\text{gap}}$ is related to the superconducting state. Its temperature variation is displayed in Fig. 3(c) and has been derived from fits to the data shown in Figs. 2(a) and 3(a) and additional scans. As indicated by the solid line, $\hbar\omega_{\text{gap}}$ follows, within the error bars, the BCS form for the superconducting gap amplitude $2\Delta(T)$.

We now turn to the momentum dependence of the magnetic response around \mathbf{Q}_{AF} in the superconducting state. Fig. 4 displays \mathbf{Q} scans along $(h\ h\ 1.458)$ across \mathbf{Q}_{AF} recorded at different energy transfers $\hbar\omega$ and at $T = 0.06\text{ K}$. The single peak seen at $\hbar\omega \approx 0.2\text{ meV}$ splits upon increasing energy transfer into two peaks which move further apart from each other along with a marked decrease in intensity. Fits with two peaks of Gaussian lineshape (solid lines) yield a good description of the data. The peak positions for different $\hbar\omega$, drawn in the inset of Fig. 4(a), yield a linear dispersion relation. We conclude that the spin excitations are part of an *overdamped dispersive* mode. Its velocity as read off the slope of the dispersion curve, $v_{\text{exc}} = (4.44 \pm 0.86)\text{ meV\AA}$, is substantially smaller than the strongly renormalised Fermi velocity $v_{\text{F}}^* \approx 57\text{ meV\AA}$ ($1\text{ meV\AA} = 153\text{ m/s}$). This indicates a retardation of the coupling between the heavy quasiparticles and the quantum-critical spin excitations.

Superconducting condensation and magnetic exchange energies

The observed spin excitations both below and above T_c allow us to estimate the decrease of magnetic exchange energy in the superconducting state as compared to the putative normal state. This saving of exchange energy is determined as follows^{21,22}:

$$\Delta E_x \equiv E_x^N - E_x^S = \frac{1}{g^2 \mu_B^2} \int_0^\infty \frac{d(\hbar\omega)}{\pi} [n(\hbar\omega) + 1] \times \left\langle I(\mathbf{q}) \left[\text{Im}\chi^N(\mathbf{q}, \omega) - \text{Im}\chi^S(\mathbf{q}, \omega) \right] \right\rangle,$$

where $E_x^{N/S}$ is respectively the exchange energy in the normal (N) and superconducting (S) states, $\langle \rangle$ indicates an average over the first Brillouin zone, and $\mathbf{q} = (q_x, q_y, q_z)$ denotes a momentum transfer in the first Brillouin zone, i.e., $\mathbf{Q} = \mathbf{G} + \mathbf{q}$. $I(\mathbf{q})$ is the exchange interaction between the localised f -moments and contains nearest (I_1) and next nearest (I_2) neighbour terms:

$$I(\mathbf{q}) = I_1[\cos(q_x a) + \cos(q_y a)] + I_2 f_2(a, c, \mathbf{q}) \quad (1)$$

where a and c are the lattice constants, and the precise form of f_2 is given in¹⁴. The inclusion of the next nearest neighbour terms is a consequence of the three-dimensional nature of the spin excitations of CeCu₂Si₂ (cf. Fig. 1(c)). This is different from the cuprate superconductors and e.g. CeCoIn₅, where the observed behaviour is predominantly two-dimensional. As described in detail in the supplementary material¹⁴, we find a magnetic exchange energy saving of $\Delta E_x = \eta 4.8 \cdot 10^{-3}$ meV per Ce ($\eta \approx 1.25$, η being a measure of the SC volume fraction¹⁴). This energy saving stems primarily from the spectrum at low energies, below the magnetic excitation gap. This follows from the fact that the spin excitations are peaked around the wave vector \mathbf{Q}_{AF} at which $I(\mathbf{q})$ is positive. Fig. 5 illustrates which part of the spectrum of $\text{Im}\chi(\mathbf{Q}_{\text{AF}}, \omega)$ increases/decreases ΔE_x . This energy gain must be compared with the superconducting condensation energy ΔE_C , which is the difference in internal energy between the (putative) normal and the superconducting state at $T = 0$ ^{21,22}:

$$\Delta E_C = U_N(T = 0) - U_S(T = 0). \quad (2)$$

Using the specific heat data shown in Fig. 6(a)¹⁴, we find the condensation energy to be $\eta 2.27 \cdot 10^{-4}$ meV per Ce. Compared to the high- T_c cuprates where similar analyses have been performed²³⁻²⁵, the considerably lower energy scales in the HF systems enable us to

perform a quantitative analysis of the data in terms of an accessible putative normal state. As noted above, extrapolating the spin excitations from above T_c is in good qualitative agreement with the excitations of the field-driven normal state at the lowest temperatures. Furthermore, the electronic specific heat of both the superconducting and normal state can be reliably determined since phonons do not contribute at such low temperatures. Despite this apparent advantage of HF systems, ΔE_C and ΔE_x have not received much attention in the context of HF SC. ΔE_C has been determined for CeCoIn_5 ¹⁰, a compound whose proximity to quantum criticality is not yet certain, since SC sets in before AF order can develop. Our study represents the first determination of the savings in both the exchange energy and condensation energy for a superconductor near an AF QCP, as well as for any unconventional low-temperature superconductor.

Our observation that the magnetic exchange energy saving is more than one order of magnitude larger than the condensation energy implies that AF excitations are the primary driving force for SC. A comparable factor of exchange energy saving over condensation energy has recently been observed in the unconventional superconductor $\text{YbBa}_2\text{Cu}_3\text{O}_{6.6}$ ²⁵. As described above, the temperature dependence of $\omega_{\text{gap}}(T)$ in CeCu_2Si_2 follows a rescaled BCS form. For a conventional BCS superconductor, where $\Theta_D \gg \omega_{\text{gap}}$, the saving in potential energy is enhanced over the condensation energy by a factor that depends logarithmically on the ratio of Debye temperature Θ_D and superconducting gap $\omega_{\text{gap}}(T=0)$ ²⁷. The corresponding enhancement factor over the condensation energy in CeCu_2Si_2 , where the Kondo temperature $T_K \approx 15$ K replaces the Debye temperature Θ_D , turns out to be two. The fact that the observed magnetic energy saving is more than a factor 20 larger than the condensation energy, indicates a large loss in kinetic energy. A natural origin for the latter lies in the Kondo effect, since the kinetic energy of the quasiparticles appears through the Kondo-interaction term. Because superconducting pairing in CeCu_2Si_2 occurs in the spin-singlet channel, the opening of the superconducting gap therefore weakens the Kondo-singlet formation and, by extension, reduces the spectral weight of the Kondo resonance¹⁴.

Comparison with other unconventional superconductors

Our understanding of the magnetic exchange energy saving in the HF superconductor CeCu_2Si_2 near its AF QCP naturally leads us to ask whether the effect is universal. SC-

induced enhancement of the spin-fluctuation spectrum in some frequency range has also been observed in the high- T_c cuprates such as $\text{YBa}_2\text{Cu}_3\text{O}_{7-\delta}$ ²⁸, iron pnictides such as K- or Co-doped BaFe_2As_2 ^{29,30} or $\text{FeTe}_{1-x}\text{Se}_x$ ^{31,32}, as well as two other HF compounds, UPd_2Al_3 ^{33,34} and CeCoIn_5 ¹⁰. However, there are some striking differences between the spectrum observed in CeCu_2Si_2 and those seen in the other superconductors. In contrast to CeCu_2Si_2 , where SC and long-range AF order exclude each other, SC in UPd_2Al_3 occurs inside the antiferromagnetically ordered part of its magnetic phase diagram, which is far away from any QCP³⁵. Whether a QCP underlies SC in the cuprates, the iron pnictides, or CeCoIn_5 , is yet to be established. The normal state magnetic response of S-type CeCu_2Si_2 at \mathbf{Q}_{AF} slows down considerably, when lowering the temperature, indicating its proximity to a QCP, and displays pronounced dispersion. CeCu_2Si_2 represents, therefore, the only system in which we can unambiguously establish the linkage between AF quantum criticality and unconventional SC, even though the effect may well prove to be broadly relevant. In comparison to other HF superconductors, the inelastic spin response in CeCu_2Si_2 is broad in energy and extends beyond 10 times the gap value, while in CeCoIn_5 a rather sharp, resolution-limited spin resonance is found¹⁰. Furthermore, unlike CeCoIn_5 the temperature dependences of the spin excitation gap in CeCu_2Si_2 and UPd_2Al_3 ³⁶ do follow the expected BCS form. In comparison to CeCu_2Si_2 , UPd_2Al_3 also exhibits a dispersive spin excitation starting at the low-energy inelastic line (related to the edge of the spin gap³⁴) with a slightly higher in-plane mode velocity³⁷. However, the situation in the cuprate superconductors is more complex, with an hour-glass like dispersion of the resonance mode³⁸⁻⁴⁰.

Experimentally the most prominent difference between CeCu_2Si_2 and other unconventional superconductors is the \mathbf{Q} position of the spin excitation gap, which is observed in all reported unconventional superconductors at or close to simple commensurate positions with half-integer indices. E.g., in UPd_2Al_3 and CeCoIn_5 it occurs at commensurate positions, $\mathbf{Q} = (0\ 0\ 1/2)$ and $(1/2\ 1/2\ 1/2)$ respectively^{10,37}. In contrast, in S-type CeCu_2Si_2 the gapped spin excitations are restricted to the vicinity of the ordering wave vector of the system, $\tau \approx (0.215\ 0.215\ 0.53)$, which is incommensurate, far away from a simple commensurate value. As a result, the opening of a spin gap becomes the major source of exchange energy saving. By extension, an additional excitonic resonance in $\chi^S(\mathbf{Q}, \omega)$ due to the superconducting state¹¹ would reduce the energy saving. This is a striking difference between CeCu_2Si_2 on the one hand, and CeCoIn_5 ¹⁰ and high- T_c cuprate superconductors²⁴ on the

other.

In conclusion, our inelastic neutron scattering experiments in CeCu_2Si_2 reveal spin excitations associated with the AF (3D-SDW) QCP. These spin excitations are overdamped, dispersive and gapped in the superconducting state. Our quantitative estimate of both, the change in magnetic exchange energy and the superconducting condensation energy identifies the AF excitations as a major driving force for SC. AF QCPs are currently being explored in a variety of strongly correlated electron systems, including the new Fe pnictide superconductors. $\text{Ba}(\text{Fe}_{1-x}\text{Co}_x)_2\text{As}_2$ ⁴², for instance, exhibits a $T - x$ phase diagram very similar to the $T - p$ phase diagram of CePd_2Si_2 , raising the prospect that AF quantum critical excitations also drive the superconducting pairing in these new high- T_c superconductors.

-
1. Steglich, F. *et al.* Superconductivity in the presence of strong Pauli paramagnetism: CeCu_2Si_2 . *Phys. Rev. Lett.* **43**, 1892–1896 (1979).
 2. Miyake, K., Schmitt-Rink, S. & Varma, C. M. Spin-fluctuation-mediated even-parity pairing in heavy-fermion superconductors. *Phys. Rev. B* **34**, 6554–6556 (1986).
 3. Scalapino, D. J., Loh, E. & Hirsch, J. E. d-wave pairing near a spin-density-wave instability. *Phys. Rev. B* **34**, 8190–8192 (1986).
 4. Monthoux, P., Pines, D. & Lonzarich, G. G. Superconductivity without phonons. *Nature* **450**, 1177–1183 (2007).
 5. Mathur, N. D. *et al.* Magnetically mediated superconductivity in heavy fermion compounds. *Nature* **394**, 39–43 (1998).
 6. Gegenwart, P., Si, Q. & Steglich, F. Quantum criticality in heavy-fermion metals. *Nat. Phys.* **4**, 186–197 (2008).
 7. Steglich, F. *et al.* *More is different – Fifty years of condensed matter physics*, chap. Superconductivity and magnetism in heavy-fermions, p. 191–210 (Princeton University Press, 2001).
 8. Gegenwart, P. *et al.* Breakup of heavy fermions on the brink of “Phase A” in CeCu_2Si_2 . *Phys. Rev. Lett.* **81**, 1501–1504 (1998).
 9. Yuan, H. Q. *et al.* Observation of two distinct superconducting phases in CeCu_2Si_2 . *Science* **302**, 2104–2107 (2003).
 10. Rosch, A. Interplay of disorder and spin fluctuations in the resistivity near a quantum critical

- point. *Phys. Rev. Lett.* **82**, 4280–4283 (1999).
11. Stockert, O. *et al.* Nature of the A phase in CeCu₂Si₂. *Phys. Rev. Lett.* **92**, 136401 (2004).
 12. Holmes, A. T., Jaccard, D. & Miyake, K. Signatures of valence fluctuations in CeCu₂Si₂ under high pressure. *Phys. Rev. B* **69**, 024508 (2004).
 13. Steglich, F. *et al.* New observations concerning magnetism and superconductivity in heavy-fermion metals. *Physica B* **223-224**, 1–8 (1996).
 14. See supplementary material on Nature physics online.
 15. Stockert, O. *et al.* Magnetism and superconductivity in the heavy-fermion compound CeCu₂Si₂ studied by neutron scattering. *Physica B* **403**, 973–976 (2008).
 16. Rauchschalbe, U. *et al.* Critical fields of the "heavy-fermion" superconductor CeCu₂Si₂. *Phys. Rev. Lett.* **49**, 1448–1451 (1982).
 17. Ohkawa, F. Cooper pairs of $d_{x^2-y^2}$ -symmetry in simple square lattices. *J. Phys. Soc. Jpn.* **56**, 2267–2270 (1987).
 18. Ishida, K. *et al.* Evolution from magnetism to unconventional superconductivity in a series of Ce_xCu₂Si₂ compounds probed by Cu NQR. *Phys. Rev. Lett.* **82**, 5353–5356 (1999).
 19. Fujiwara, K. *et al.* High pressure NQR measurement in CeCu₂Si₂ up to sudden disappearance of superconductivity. *J. Phys. Soc. Jpn.* **77**, 123711 (2008).
 20. Stockert, O. *et al.* Peculiarities of the antiferromagnetism in CeCu₂Si₂. *J. Phys.: Conf. Ser.* **51**, 211–218 (2006).
 21. Scalapino, D. J. & White, S. R. Superconducting condensation energy and an antiferromagnetic exchange-based pairing mechanism. *Phys. Rev. B* **58**, 8222–8224 (1998).
 22. Leggett, A. Where is the energy saved in cuprate superconductivity? *J. Phys. Chem. Solids* **59**, 1729–1732 (1998).
 23. Demler, E. & Zhang, S.-C. Quantitative test of a microscopic mechanism of high-temperature superconductivity. *Nature* **396**, 733–735 (1998).
 24. Woo, H. *et al.* Magnetic energy change available to superconducting condensation in optimally doped YBa₂Cu₃O_{6.95}. *Nat. Phys.* **2**, 600–604 (2006).
 25. Dahm, T. *et al.* Strength of the spin-fluctuation-mediated pairing interaction in a high-temperature superconductor. *Nat. Phys.* **5**, 217–221 (2009).
 26. Stock, C., Broholm, C., Hudis, J., Kang, H. J. & Petrovic, C. Spin resonance in the d-wave superconductor CeCoIn₅. *Phys. Rev. Lett.* **100**, 087001 (2008).

27. Haslinger, R. & Chubukov, A. V. Condensation energy in strongly coupled superconductors. *Phys. Rev. B* **68**, 214508 (2003).
28. Sidis, Y. *et al.* Magnetic resonant excitations in high- T_c superconductors. *phys. status solidi b* **241**, 1204–1210 (2004).
29. Christianson, A. D. *et al.* Unconventional superconductivity in $\text{Ba}_{0.6}\text{K}_{0.4}\text{Fe}_2\text{As}_2$ from inelastic neutron scattering. *Nature* **456**, 930–932 (2008).
30. Inosov, D. S. *et al.* Normal-state spin dynamics and temperature-dependent spin-resonance energy in optimally doped $\text{BaFe}_{1.85}\text{Co}_{0.15}\text{As}_2$. *Nat. Phys.* **6**, 178–181 (2010).
31. Qiu, Y. *et al.* Spin gap and resonance at the nesting wave vector in superconducting $\text{FeSe}_{0.4}\text{Te}_{0.6}$. *Phys. Rev. Lett.* **103**, 067008 (2009).
32. Lumsden, M. D. *et al.* Evolution of spin excitations into the superconducting state in $\text{FeTe}_{1-x}\text{Se}_x$. *Nat. Phys.* **6**, 182–186 (2010).
33. Bernhoeft, N. *et al.* Enhancement of magnetic fluctuations on passing below T_c in the heavy fermion superconductor UPd_2Al_3 . *Phys. Rev. Lett.* **81**, 4244–4247 (1998).
34. Sato, N. K. *et al.* Strong coupling between local moments and superconducting 'heavy' electrons in UPd_2Al_3 . *Nature* **410**, 340–343 (2001).
35. Link, P., Jaccard, D., Geibel, C., Wassilew, C. & Steglich, F. The heavy-fermion superconductor UPd_2Al_3 at very high pressure. *J. Phys.: Condens. Matter* **7**, 373–378 (1995).
36. Bernhoeft, N. *et al.* Magnetic fluctuations above and below T_c in the heavy fermion superconductor UPd_2Al_3 . *Physica B* **259-261**, 614–620 (1999).
37. Hiess, A. *et al.* Magnetization dynamics in the normal and superconducting phases of UPd_2Al_3 : I. surveys in reciprocal space using neutron inelastic scattering. *J. Phys.: Condens. Matter* **18**, R437–R451 (2006).
38. Pailhès, S. *et al.* Resonant magnetic excitations at high energy in superconducting $\text{YBa}_2\text{Cu}_3\text{O}_{6.85}$. *Phys. Rev. Lett.* **93**, 167001 (2004).
39. Hayden, S. M., Mook, H. A., Dai, P., Perring, T. G. & Dogan, F. The structure of the high-energy spin excitations in a high-transition-temperature superconductor. *Nature* **429**, 531–534 (2004).
40. Tranquada, J. M. *et al.* Quantum magnetic excitations from stripes in copper oxide superconductors. *Nature* **429**, 534–538 (2004).
41. Eremin, I., Zwicky, G., Thalmeier, P. & Fulde, P. Feedback spin resonance in supercon-

- ducting CeCu₂Si₂ and CeCoIn₅. *Phys. Rev. Lett.* **101**, 187001 (2008).
42. Chu, J.-H., Analytis, J. G., Kucharczyk, C. & Fisher, I. R. Determination of the phase diagram of the electron-doped superconductor Ba(Fe_{1-x}Co_x)₂As₂. *Phys. Rev. B* **79**, 014506 (2009).
43. Wiebe, C. R. *et al.* Gapped itinerant spin excitations account for missing entropy in the hidden-order state of URu₂Si₂. *Nat. Phys.* **3**, 96–99 (2007).

Author contributions

H.S.J. and C.G. synthesised the sample. O.S., J.A., E.F., M.L., K.S. and W.S. performed the measurements. O.S., J.A. and S.K. analysed the data. S.K. and Q.S. carried out theoretical calculations. O.S., S.K., Q.S. and F.S. wrote the manuscript. O.S., S.K. and F.S. planned and managed the project.

Additional information

The authors declare that they have no competing financial interests. Supplementary information accompanies this paper on www.nature.com/naturephysics. Reprints and permissions information is available online at <http://npg.nature.com/reprintsandpermissions>. Correspondence and requests for materials should be addressed to O.S.

Acknowledgements

We greatly acknowledge helpful discussions with A. Chubukov, P. Coleman, T. Dahm, I. Eremin, B. Fåk, A. Hiess and P. Thalmeier. This work was supported by the Deutsche Forschungsgemeinschaft through Forschergruppe 960 "Quantum phase transitions", as well as by the NSF Grant No. DMR-0424125 and the Robert A. Welch Foundation Grant No. C-1411.

Methods

High-resolution inelastic neutron scattering experiments were performed on the cold-neutron triple-axis spectrometer IN12 at the high-flux reactor of the Institut Laue-Langevin

in Grenoble/France. A vertical focusing graphite (002) monochromator and a doubly focused (vertical and horizontal) graphite (002) analyzer were used. The horizontal collimation was given by the neutron guide in front of the monochromator and 60' before the sample, while no collimation was inserted in the scattered beam. A liquid-nitrogen cooled Be filter was placed in the incident neutron beam to reduce higher-order contamination. The measurements were carried out with a fixed final wave vector $k_f = 1.15 \text{ \AA}^{-1}$ which corresponds to a final neutron energy $E_f = 2.74 \text{ meV}$ and yields a high energy resolution $\Delta E \approx 57 \mu\text{eV}$ (FWHM, i.e., full width at half maximum). All experiments were performed on an S-type CeCu_2Si_2 single crystal ($m \approx 2 \text{ g}$). The crystal was mounted with the $[1\bar{1}0]$ axis vertical on a copper pin attached to the mixing chamber of a dilution refrigerator. The setup results in a $[110] - [001]$ scattering plane. Data were taken at temperatures between $T = 0.06 \text{ K}$ and 1.7 K and in magnetic fields up to $B = 2.5 \text{ T}$ applied along the vertical $[1\bar{1}0]$ axis. The inelastic neutron scattering measurements were converted to units of $\mu_B^2/(\text{meV f.u.})$ by normalizing the intensities to the incoherent scattering of the sample.

Supplementary Material for “Magnetically driven superconductivity in CeCu₂Si₂”

O. Stockert¹, J. Arndt¹, E. Faulhaber^{2,3}, C. Geibel¹, H. S. Jeevan^{1,4}, S. Kirchner^{1,6}, M. Loewenhaupt², K. Schmalzl⁵, W. Schmidt⁵, Q. Si⁷, F. Steglich¹

¹ Max Planck Institute for Chemical Physics of Solids, Nöthnitzer Str. 40, 01187 Dresden, Germany

² Institut für Festkörperphysik, Technische Universität Dresden, 01062 Dresden, Germany

³ Gemeinsame Forschergruppe Helmholtz-Zentrum Berlin - TU Dresden, 85747 Garching, Germany

⁴ I. Physikalisches Institut, Universität Göttingen, 37077 Göttingen, Germany

⁵ Jülich Centre for Neutron Science at Institut Laue-Langevin, 38042 Grenoble, France

⁶ Max Planck Institute for the Physics of Complex Systems, Nöthnitzer Str. 38, 01187 Dresden, Germany

⁷Department of Physics and Astronomy, Rice University, Houston, Texas 77005-1892, USA

Sample characterization

The present neutron scattering experiments were complemented by bulk measurements on the same S-type CeCu₂Si₂ single crystal. The heat capacity was recorded using a compensated heat-pulse technique, while the ac susceptibility was measured with a homemade susceptibility setup and was recorded during the neutron scattering experiment simultaneously while the neutron data were taken. As shown in Fig. 6(a) the specific heat, plotted as C/T vs. T , exhibits a pronounced maximum indicating the onset of superconductivity at $T_c = 0.6$ K. The shape of the anomaly at T_c in comparison to heat capacity measurements on other CeCu₂Si₂ samples^{1,2} and its full suppression already in a magnetic field of $B = 2$ T clearly indicate that this is a transition into the superconducting state. The superconducting nature of this phase transition is further confirmed by ac susceptibility measurements displayed in Figs. S1(b) and (c). A sharp drop of $\chi_{ac}(T)$ at $T_c \approx 600$ mK is observed with a large diamagnetic signal at lower temperatures. Furthermore, the susceptibility measurements yield an upper critical magnetic field B_{c2} to kill superconductivity of $B_{c2} = 1.7$ T for $B \parallel [1\bar{1}0]$ at $T = 0.07$ K.

From entropy the single-ion Kondo temperature T_K was deduced to almost coincide with

the lattice coherence temperature as obtained from the position of the low-temperature peak in the temperature dependence of the electrical resistivity³. Both are around 15 K. From the Doniach criterion together with the fact that our sample is almost quantum critical it follows that the magnetic energy scale $T_{\text{RKKY}} \approx T_{\text{K}} \approx 15$ K.

Analysis of magnetic response

The neutron intensity is directly proportional to the scattering function $S(\mathbf{Q}, \omega)$. In the paramagnetic, normal state of S-type CeCu₂Si₂ the magnetic response was fitted by a quasielastic signal with Lorentzian lineshape (cf. Figs. 2(a) and (b) and Fig. 3(a)). Hence, the scattering function $S(\mathbf{Q}, \omega)$ at momentum transfer $\hbar\mathbf{Q}$ and energy transfer $\hbar\omega$ takes the form

$$S_{qe,mag}(\mathbf{Q}, \omega) = [n(\hbar\omega) + 1] \cdot \text{Im}\chi(\mathbf{Q}, \omega) = [n(\hbar\omega) + 1] \cdot \frac{\hbar\omega\chi_0}{\pi\Gamma} \cdot \frac{1}{1 + (\hbar\omega/\Gamma)^2},$$

at temperature T where $n(\hbar\omega) + 1 = 1/[1 - \exp(-\hbar\omega/kT)]$ is the Bose factor and k is Boltzmann constant. Here, χ_0 denotes the susceptibility and Γ the energy linewidth of the fluctuations (HWHM, half width at half maximum), which is inversely proportional to the lifetime τ of the fluctuations. In the superconducting state the magnetic response was modeled using a modified scattering function taking the electronic density of states in a superconductor, $Z(\omega)$, into account, i.e.,

$$Z(\omega) = \begin{cases} \frac{\omega}{\sqrt{\omega^2 - \omega_{gap}^2}} & \text{for } \omega \geq \omega_{gap} \\ 0 & \text{otherwise.} \end{cases}$$

$\omega_{gap} = \omega_{gap}(T)$ is the value of the superconducting gap at a certain temperature T . $S_{ine,mag}(\mathbf{Q}, \omega) = S_{qe,mag}(\mathbf{Q}, \omega) \cdot Z(\omega)$ was then used to describe the data in the superconducting state (cf. Figs. 2(a), (b) and 3(a)). In each case the scattering function was convolved with the instrumental resolution to fit the experimental data.

Determination of condensation and magnetic exchange energies

The condensation energy ΔE_C characterises the stability of the superconducting state (S) against a putative normal state (N) and is the difference in internal energy, or

$$\lim_{T \rightarrow 0} (G_N(T, B = 0) - G_S(T, B = 0)) = \mu_0 V \int_0^{B_c^2} M(T = 0) dB = \frac{1}{2} \mu_0 V B_c^2, \quad (\text{S3})$$

where G_S/G_N is the Gibbs free energy of the superconducting (S)/normal (N) state and B_c is the thermodynamic critical field defined via $\frac{1}{2} B_c^2 \equiv \int_0^{B_c^2} M dH$. For CeCu₂Si₂, B_c has been determined in Ref.⁴. However, the co-existence of small, magnetically ordered regions in the superconducting S-type CeCu₂Si₂ makes it necessary to perform all energy estimates on the same sample. Eq.(S3) implies that ΔE_C can be obtained from the specific heat data of Fig. 6(a):

$$\begin{aligned} \Delta E_C &= \int_0^{T_c} dT \int_0^T dT' \frac{1}{T'} (C_V^N(T') - C_V^S(T')) \\ &= \eta 431 \text{ J/m}^3 = \eta 2.27 \cdot 10^{-4} \text{ meV/Ce}. \end{aligned} \quad (\text{S4})$$

Here and in what follows, we take the finite field ($B = 2 \text{ T}$) data as the putative normal state. From the lowest temperature ($T < 0.1 \text{ K}$) the data were extrapolated to $T = 0$ and the contribution from the nuclear moments was subtracted. The contribution from below $T = 0.1 \text{ K}$ to ΔE_C is tiny ($\Delta E_C^{T < 0.1 \text{ K}} = \eta 7.6 \text{ J/m}^3 = \eta 4 \cdot 10^{-6} \text{ meV/Ce}$). The factor $\eta > 1$ accounts for the fact that only the superconducting volume fraction ($1/\eta$) contributes to ΔE_C , and it may very well be sample dependent.

We now turn to estimating the difference in exchange energy between the normal and superconducting states, in order to ascertain whether the magnetic excitations contribute significantly to the condensation energy. Heavy-fermion metals are best described by the Anderson lattice model⁵. To estimate the magnetic exchange energy in such a system, it is sufficient to consider the magnetic limit of the Anderson lattice model, i.e., the Kondo lattice model:

$$H_{KL} = \sum_{\mathbf{k}, \sigma} \epsilon_{\mathbf{k}} c_{\mathbf{k}\sigma}^\dagger c_{\mathbf{k}\sigma} + J_K \sum_i \mathbf{S}_i \cdot \mathbf{s}_c(\mathbf{r}_i), \quad (\text{S5})$$

where \mathbf{S}_i is the localised moment at a cerium site \mathbf{r}_i which is coupled via the Kondo coupling J_K to the spd conduction electron spin density $\mathbf{s}_c(\mathbf{r}_i)$ at the cerium site, and $\epsilon_{\mathbf{k}}$ describes the conduction electron bandstructure. The Kondo model describes not only the formation

of heavy quasiparticles but also the AF phase and the quantum critical point, since H_{KL} implicitly contains the RKKY interaction among the Ce moments:

$$H_{RKKY} = \sum_{i < j} I_{i,j} \mathbf{S}_i \cdot \mathbf{S}_j, \quad (\text{S6})$$

where the exchange constants $I_{i,j} \sim J_K^2$.

We model the exchange interaction between the localised Ce-moments by including nearest neighbour and next nearest neighbour terms appropriate for the tetragonal, body-centred unit cell:

$$\begin{aligned} I(\mathbf{q}) = & I_1 [\cos(q_x a) + \cos(q_y a)] + I_2 [\cos(q_x a/2 + q_y a/2 + q_z c/2) \\ & + \cos(-q_x a/2 + q_y a/2 + q_z c/2) + \cos(-q_x a/2 - q_y a/2 + q_z c/2) \\ & + \cos(q_x a/2 - q_y a/2 + q_z c/2) + \cos(p_x a + p_y a) + \cos(p_y a - p_x a)], \end{aligned} \quad (\text{S7})$$

where $a = 4.1 \text{ \AA}$ and $c = 9.9 \text{ \AA}$ are the lattice constants for the a - and c -axis, respectively and I_1 and I_2 are the nearest and next nearest neighbour exchange interactions. The energy saving in magnetic exchange energy of the superconducting ground state compared to the putative normal ground state is then given by

$$\begin{aligned} \Delta E_x \equiv E_x^N - E_x^S = & \frac{A}{g^2 \mu_B^2} \int_0^\infty \frac{d(\hbar\omega)}{\pi} [n(\hbar\omega) + 1] \\ & \times \int_{-\pi/a}^{\pi/a} dq_x \int_{-\pi/a}^{\pi/a} dq_y \int_{-\pi/c}^{\pi/c} dq_z I(q_x, q_y, q_z) \\ & \times \text{Im} \left[\chi^N(q_x, q_y, q_z, \hbar\omega) - \chi^S(q_x, q_y, q_z, \hbar\omega) \right] \Bigg/ \int_{-\pi/a}^{\pi/a} dq_x \int_{-\pi/a}^{\pi/a} dq_y \int_{-\pi/c}^{\pi/c} dq_z. \end{aligned} \quad (\text{S8})$$

Crystalline-electric-field effects split the $J = 5/2$ states of the Ce^{3+} ion up into a ground-state doublet and a quasi-quartet at high energies ($> 30 \text{ meV}$) and result in $g_z \approx g_\perp \approx 2$, and an almost isotropic spin susceptibility⁶. A is a constant given by $A = \eta \cdot 8 \cdot 3/2$ resulting from the eight symmetry equivalent incommensurate AF wave vectors in the first Brillouin zone and the fact that neutrons only detect moments and spin fluctuations perpendicular to the actual momentum transfer. Our sign convention in Eq. (S3) implies that a positive ΔE_x is equivalent to an energy saving in the superconducting state. Different energy ranges will in general contribute differently in either decreasing or increasing the exchange energy as the system goes from the (putative) $T=0$ normal state to the superconducting state.

The exchange constants I_1 and I_2 of Eq. (S7) follow from three independent relations: (i) the observed dispersion of Fig. 7(a), (ii) the fact that S-type CeCu₂Si₂ is close to quantum criticality and meets the Doniach criterion and (iii) the functional form of the RKKY interaction. To estimate the magnitude of the exchange interaction I_1 , we chose v_{exc} from the observed dispersion of the overdamped excitations (see inset of Fig. 4(a)). Using the mean field expression of v_{exc} for a three-dimensional, cubic lattice with $I_2 = 0$, we find $I_1 = 0.63 \text{ meV}$. Note, that an $I_2 > 0$ will lead to an increase in I_1 for fixed dispersion, making $I_1 = 0.63 \text{ meV}$ an estimate from below. Alternatively, estimating I_1 via the Doniach criterion, we find that $I_1 \approx 0.6 \text{ meV}$ when using $T_K \approx 15 \text{ K}$ and the fact that S-type CeCu₂Si₂ is almost quantum critical. The ratio I_1/I_2 is estimated from the distance-dependence of the RKKY interaction. This interaction shows oscillatory behaviour with an envelope that falls off as a function of the inverse of the distance r between the Ce moments. For free electrons, this function is a simple power law and the period of the oscillating function is set by $2k_F r$. In CeCu₂Si₂, the RKKY interaction is mediated by the spd conduction electrons. For a reliable estimate of the ratio I_1/I_2 in CeCu₂Si₂ we combine band structure calculations for the non-magnetic La-homologue LaCu₂Si₂ of reference⁷ with the RKKY interaction for non-spherical Fermi surfaces obtained by L. Roth et al.⁸. As found by Roth et al., the RKKY interaction shows a $1/r^3$ dependence even for non-spherical Fermi surfaces except for directions where the effective band mass diverges. We therefore set $I_1/I_2 \approx r_2^3 \cos(\phi_1)/(r_1^3 \cos(\phi_2))$ or $I_2 \approx 0.35 I_1 \cos(\phi_2)/\cos(\phi_1)$, where r_1 (r_2) is the distance between nearest (next nearest) neighbour Ce atoms and $\cos(\phi_1)$ and $\cos(\phi_2)$ are oscillating factors which not only depend on the magnitude of r_1/r_2 but also on the direction for non-spherical Fermi surfaces. The oscillating factors are determined by the wave vector differences of caliper pairs of points of the Fermi surface along the [110] for the next nearest neighbour in the basal plane and [111] directions for the next nearest neighbour in the unit cell centre^{7,8}.

As a result, the next nearest neighbour exchange constant $I_2^{\text{basal}} = -0.08 I_1$ for two Ce moments in the basal plane differs from the exchange constant $I_2^{\text{center}} = 0.60 I_1$ for next nearest neighbours in the unit cell centres. We are only interested in a lower estimate for the exchange energy gain and use a simple average $I_2 = (I_2^{\text{basal}} + 2I_2^{\text{center}})/3 \approx 0.38 I_1$ for the next nearest neighbour exchange constant in Eq. (S7). Note that there are twice as many next nearest neighbours in the unit cell centre than in the basal plane.

The volume fraction η enters Eq. (S8), since the magnetically ordered regions in S and N yield (essentially) identical responses for $B = 0$ and $B = 2$ T. Therefore, the actual change in exchange energy between S and N is larger by a factor η . As a result, the ratio between ΔE_C and ΔE_x will be independent of η . Nonetheless, an estimate of the volume fraction η of our sample can be obtained from the ordered moment associated with the elastic magnetic response and the weak anomaly in the heat capacity yielding $\approx 0.02 \mu_B/\text{Ce}$. Comparing this to the ordered moment in the A-phase, $\mu_{ord} \approx 0.1 \mu_B/\text{Ce}$ yields $\eta \approx 1.25$.

The spin susceptibility in the normal state has been parametrized as

$$\text{Im}\chi^N(\mathbf{Q}, \omega) = \frac{\chi_0}{1 + \xi^2(\mathbf{Q} - \mathbf{Q}_{\text{AF}})^2} \frac{\hbar\omega/\Gamma_q}{1 + (\hbar\omega/\Gamma_q)^2} \quad (\text{S9})$$

$$= \frac{\chi_0}{1 + (\xi/a)^2(a(Q_x - Q_{\text{AF}}^x))^2 + (\xi/a)^2(a(Q_y - Q_{\text{AF}}^y))^2 + (\xi/c)^2(c(Q_z - Q_{\text{AF}}^z))^2} \frac{2\hbar\omega/\Gamma}{1 + 4(\hbar\omega/\Gamma)^2}.$$

In the superconducting state, the susceptibility has been modeled as

$$\text{Im}\chi^S(\mathbf{Q}, \omega) = \frac{\omega}{\sqrt{\omega^2 - \omega_{\text{gap}}^2}} \text{Im}\chi^N(\mathbf{Q}, \omega), \quad (\text{S10})$$

for $\omega \geq \omega_{\text{gap}}$ and zero otherwise. These expressions model very well the experimental data for $\text{Im}\chi^N(\mathbf{Q}, \omega)$ and $\text{Im}\chi^S(\mathbf{Q}, \omega)$ in the vicinity of \mathbf{Q}_{AF} at small energy transfers where ω_{gap} is independent of \mathbf{Q} . Away from \mathbf{Q}_{AF} and at energy transfers above 0.5 meV $\text{Im}\chi^N(\mathbf{Q}, \omega)$ and $\text{Im}\chi^S(\mathbf{Q}, \omega)$ are identical (within the experimental error bars) and therefore do not contribute to ΔE_x .

Putting everything together, we obtain $\Delta E_x = \eta 4.8 \cdot 10^{-3} \text{ meV/Ce}$ and $\Delta E_x/\Delta E_C = 21.1$. The parameters in Eq.(S9) and (S10) were obtained from fits to the experimental data at $T = 0.07$ K in the superconducting ($B = 0$) and normal ($B = 2$ T) state as $\xi = 20 - 25 \text{ \AA}$, $\Gamma_N = 0.11 \text{ meV}$, $\chi_0^N = 15.64 \mu_B^2$, $\Gamma_S = 0.225 \text{ meV}$, and $\chi_0^S = 8.69 \mu_B^2$. We checked that the associated static structure factors integrated over the full Brillouin zone (“local moment sum rule”) in the normal and superconducting state yield identical results (within a 5% error). The (in reciprocal space) isotropic fit to $\text{Im}\chi^N$ ($\text{Im}\chi^S$), see⁹, suggests that the value for ΔE_x is an estimate from below. We also checked that even if I_2 were zero, ΔE_x would still be one order of magnitude larger than ΔE_C .

A realistic modelling of the dynamic susceptibility of the normal and superconducting states in the entire momentum and frequency range should include the overdamped, dispersive excitations. This can be accomplished by parameterising the normal state susceptibility

by the SDW form

$$\chi(\mathbf{Q}, \omega) = \frac{\chi_0}{1 + \xi^2(\mathbf{Q} - \mathbf{Q}_{AF})^2 - b^2\xi^2\omega^2 - i\xi^2\omega/\Gamma} \quad (\text{S11})$$

which includes an overdamped excitation at

$$\omega = \omega_{exc} = \pm b^{-1} \sqrt{\xi^{-2} + (\mathbf{Q} - \mathbf{Q}_{AF})^2} \quad (\text{S12})$$

where ξ is the correlation length and $b = v_{exc}^{-1}$ follows from the dispersion relation of Fig. 4(a). Eq. (S11) reproduces the observed Lorentzian lineshape of the overdamped, dispersive mode for a fixed ω and $\mathbf{Q} \sim \mathbf{Q}_{exc}$ (where \mathbf{Q}_{exc} is a solution to Eq. (S12)):

$$\text{Im}\chi^N(\mathbf{Q}, \omega) = \frac{1}{\pi} \frac{\tilde{\chi}_0\omega/\tilde{\Gamma}}{(\mathbf{Q} - \mathbf{Q}_{exc})^2 + \omega^2/\tilde{\Gamma}^2}, \quad (\text{S13})$$

where $\tilde{\Gamma} = 2\Gamma|\mathbf{Q}_{AF} - \mathbf{Q}_{exc}|$ and $\tilde{\chi}_0 = \pi/(2\xi^2|\mathbf{Q}_{AF} - \mathbf{Q}_{exc}|)$. Fitting the \mathbf{Q} -dependence of the data at different energies gives rise to the same width, as required by Eq. (S13). $\text{Im}\chi^N(\mathbf{Q}, \omega)$ and $\text{Im}\chi^S(\mathbf{Q}, \omega)$ are identical at energy transfers above 0.5 meV and are still sizeable in magnitude for \mathbf{Q} sufficiently away from \mathbf{Q}_{AF} . We found that the best fit to the superconducting $\text{Im}\chi^S$ could be obtained from

$$\text{Im}\chi^S(\mathbf{Q}, \omega) = \Theta(\omega_{gap} - \omega) \frac{\omega}{(\omega^3 - \omega_{gap}^3)^{1/3}} \text{Im}\chi^N(\mathbf{Q}, \omega). \quad (\text{S14})$$

Taking $\chi_0^N = 7.0 \mu_B^2$, $\Gamma^N = 25 \text{ meV}\text{\AA}^2$ and $\chi_0^S = 6.9 \mu_B^2$, $\Gamma^S = 25 \text{ meV}\text{\AA}^2$ reproduces all features of our data (cf. Fig. 7) and results in a saving in exchange energy $\Delta E_x = \eta 4.7 \cdot 10^{-3} \text{ meV/Ce}$. The slightly modified parameters $\chi_0^N = 10.0 \mu_B^2$, $\Gamma^N = 20.0 \text{ meV}\text{\AA}^2$ and $\chi_0^S = 10.0 \mu_B^2$, $\Gamma^S = 20.0 \text{ meV}\text{\AA}^2$ capture the broad features in $\text{Im}\chi(\mathbf{Q}, \omega)$ and result in a fit of somewhat lesser quality to the data, but still yield $\Delta E_x = \eta 4.1 \cdot 10^{-3} \text{ meV/Ce}$. We therefore conclude that $\Delta E_x \gg \Delta E_C$ is a stable observation insensitive to the details of the fitting and results primarily from the changes of $\text{Im}\chi(\mathbf{Q}, \omega)$ at low energy transfers in the vicinity of \mathbf{Q}_{AF} as superconductivity sets in. The saving in exchange energy is more than an order of magnitude larger than the condensation energy, thus identifying the build up of magnetic correlations near the AF QCP as the major driving force for SC in CeCu_2Si_2 . It is important to note, that an increase in ΔE_x comes from the opening of the spin gap and not the 'resonance'-like feature above the spin gap, which tends to reduce the energy saving as illustrated in Fig. 5. This figure shows the difference of $\text{Im}\chi^S$ and $\text{Im}\chi^N$. The

blue area marked with a '+' contributes to an increase in ΔE_x whereas the green area leads to a reduction in ΔE_x , as a consequence of $I(\mathbf{Q}_{AF}) > 0$ and similar for the other wave vectors as follows from Eq. (S9). For e.g. CeCoIn_5 ^{10,11}, the shifted spectral weight in the superconducting state has to be such that the resulting positive (since $I(\mathbf{Q}) > 0$) green area exceeds the blue area for an overall saving in exchange energy. Therefore, the spin resonance at low energies observed in CeCoIn_5 and in the cuprates contributes to an increase in ΔE_x . A sharp resonance occurs in response to the superconducting state in predominantly two-dimensional superconductors and adds to a saving in exchange energy. It is however not expected in CeCu_2Si_2 , which is a 3D superconductor as deduced from the nearly isotropic upper critical field³. Instead, as shown in e.g. Figure 2(a), the magnetic response in CeCu_2Si_2 is broad and extends to more than ten times the gap energy in contrast to e.g. CeCoIn_5 or the cuprates where a sharp spin resonance has been observed.

Our results imply that there is a sizeable “kinetic” energy loss in CeCu_2Si_2 . As described in the main text, superconductivity in CeCu_2Si_2 occurs in the spin-singlet channel. As a result of the opening of the superconducting gap, the Kondo-singlet formation is weakened and the spectral weight of the Kondo resonance is reduced. The spectral weight sum rule dictates that the integration of the single-electron density of states over all energies is unchanged (and is equal to one). As a result, the lost spectral weight from low energies (within the scale of the Kondo temperature) must be transferred to higher energies, on the order of the on-site Coulomb interactions among the f -electrons where the incoherent f -electron excitations reside. This energy loss in a heavy fermion superconductor should therefore be distinguished from the ordinary kinetic energy loss of a classical superconductor¹².

-
1. Steglich, F. *et al.* Superconductivity in the presence of strong Pauli paramagnetism: CeCu_2Si_2 . *Phys. Rev. Lett.* **43**, 1892–1896 (1979).
 2. Steglich, F. *et al.* New observations concerning magnetism and superconductivity in heavy-fermion metals. *Physica B* **223-224**, 1–8 (1996).
 3. Assmus, W. *et al.* Superconductivity in CeCu_2Si_2 single crystals. *Phys. Rev. Lett.* **52**, 469–472 (1984).
 4. Rauchschalbe, U. *et al.* Critical fields of the “heavy-fermion” superconductor CeCu_2Si_2 .

- Phys. Rev. Lett.* **49**, 1448–1451 (1982).
5. Hewson, A. C. *The Kondo problem to Heavy Fermions* (Cambridge University Press, Cambridge, 1993).
 6. Goremychkin, E. A. & Osborn, R. Crystal-field excitations in CeCu_2Si_2 . *Phys. Rev. B* **47**, 14280–14290 (1993).
 7. Jarlborg, T., Braun, H. & Peter, M. Structural properties and band structure of heavy fermion systems: CeCu_2Si_2 and LaCu_2Si_2 . *Z. Phys. B* **52**, 295–301 (1983).
 8. Roth, L., Zeiger, H. & Kaplan, T. Generalization of the Ruderman-Kittel-Kasuya-Yosida Interaction for nonspherical Fermi surfaces. *Phys. Rev.* **149**, 519–525 (1966).
 9. Stockert, O. *et al.* Nature of the A phase in CeCu_2Si_2 . *Phys. Rev. Lett.* **92**, 136401 (2004).
 10. Stock, C., Broholm, C., Hudis, J., Kang, H. J. & Petrovic, C. Spin resonance in the d-wave superconductor CeCoIn_5 . *Phys. Rev. Lett.* **100**, 087001 (2008).
 11. Eremin, I., Zwicknagl, G., Thalmeier, P. & Fulde, P. Feedback spin resonance in superconducting CeCu_2Si_2 and CeCoIn_5 . *Phys. Rev. Lett.* **101**, 187001 (2008).
 12. Kirchner, S. & Si, Q. To be published.

Figures

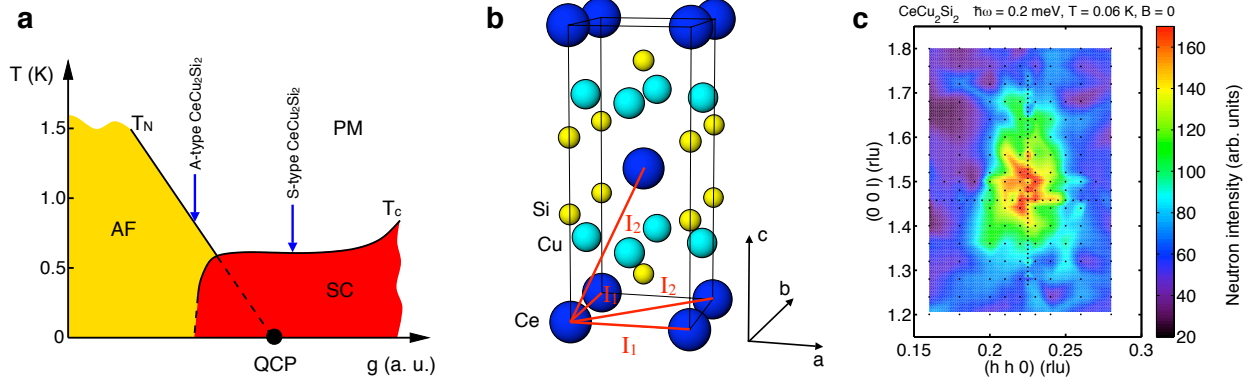


FIG. 1: **Schematic phase diagram around the QCP, crystal structure and nearly isotropic spin fluctuations of CeCu_2Si_2 .** (a) Schematic $T - g$ phase diagram of CeCu_2Si_2 in the vicinity of the quantum critical point (QCP) where the antiferromagnetic (AF) phase vanishes as function of the effective coupling constant g . Superconductivity (SC) is observed around the QCP and extends far into the paramagnetic (PM) regime. Composition as well as hydrostatic pressure can be used to change the coupling constant g and to tune the system to the QCP. The positions of the A-type and the S-type single crystals in the phase diagram are marked. (b) Tetragonal crystal structure (space group: $I4/mmm$) of CeCu_2Si_2 . The nearest and next-nearest neighbour interactions between the cerium atoms are labelled by I_1 and I_2 . It should be noted that the distances between next-nearest neighbour Ce atoms in the basal plane and out-of-plane are almost identical. (c) The spin fluctuations at $T = 0.06$ K and $B = 0$ and at an energy transfer $\hbar\omega = 0.2$ meV. The anisotropy factor between the $[110]$ and the $[001]$ directions is about 1.5. Note that the correct aspect ratio $[110]^* : [001]^*$ has been taken into account although the axes are labelled in reciprocal lattice units (rlu). Black dots mark the (\mathbf{Q}, ω) positions data were taken.

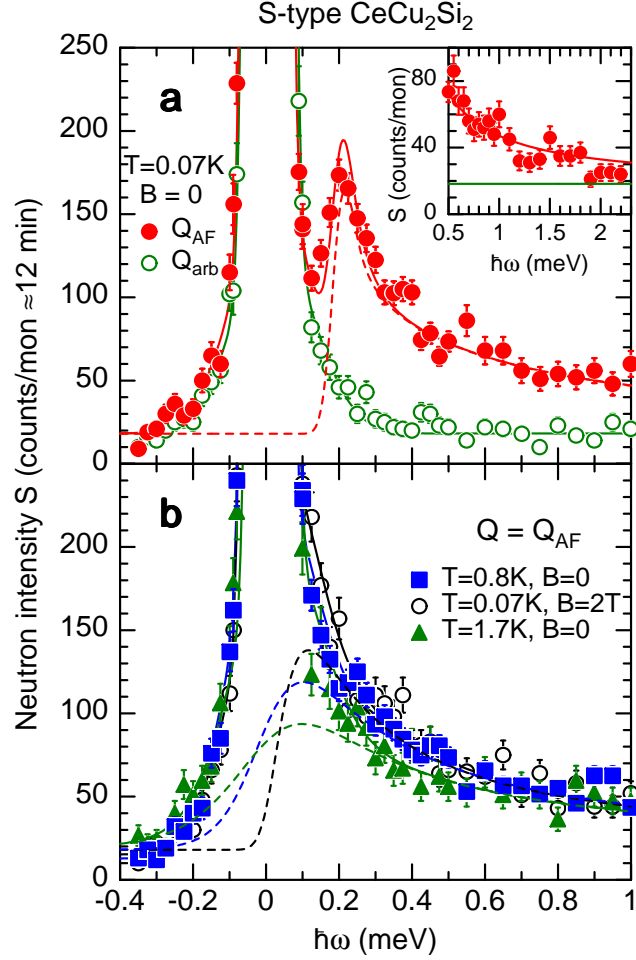


FIG. 2: Inelastic neutron scattering spectra in the normal and superconducting states of CeCu_2Si_2 . Energy scans (neutron intensity $S = S_{ela} + S_{qe/ine,mag}$ versus energy transfer $\hbar\omega$) in S-type CeCu_2Si_2 at $\mathbf{Q} = \mathbf{Q}_{AF} = (0.215 \ 0.215 \ 1.458)$ in (a) the superconducting state at $T = 0.07 \text{ K}$, $B = 0$ and in (b) the normal state at $T = 0.8$ and 1.7 K , $B = 0$ and $T = 0.07 \text{ K}$, $B = 2 \text{ T}$. For comparison the magnetic response at an arbitrary, general \mathbf{Q} position $\mathbf{Q} = \mathbf{Q}_{arb} = (0.1 \ 0.1 \ 1.6)$ at $T = 0.07 \text{ K}$, $B = 0$ is also plotted in (a). The inset in (a) shows the magnetic response at \mathbf{Q}_{AF} ($T = 0.07 \text{ K}$, $B = 0$) extending beyond $\hbar\omega = 2 \text{ meV}$. Solid lines represent fits to the data comprised of the incoherent and coherent elastic signal S_{ela} and the quasielastic/gapped inelastic magnetic response $S_{qe/ine,mag}$ (dashed lines) with Lorentzian lineshape convolved with the resolution. The gapped magnetic response at $T = 0.07 \text{ K}$, $B = 0$ has been modelled by a quasielastic Lorentzian line taking into account a spin gap with a value $\hbar\omega_{gap}$ and an enhanced density of states above the gap as for the electronic gap of a BCS superconductor. The error bars represent the statistical error.

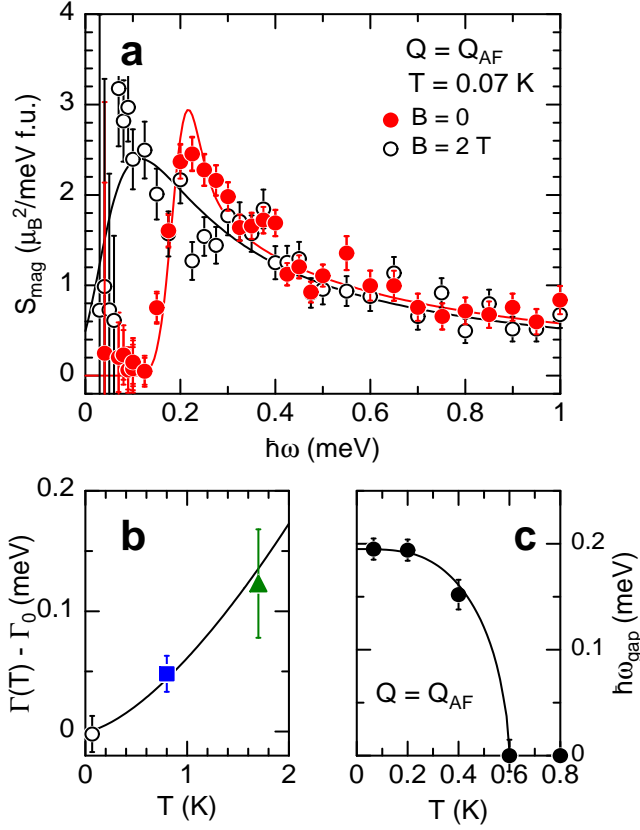


FIG. 3: **Magnetic response, relaxation rate and spin gap at the AF wave vector of CeCu_2Si_2 .** (a) Magnetic response $S_{qe/ine,mag}$ at Q_{AF} and $T = 0.07$ K in the superconducting and the normal state, i.e., at $B = 0$ and $B = 2$ T, as extracted from the data displayed in Fig. 2. The data have been put on an absolute intensity scale¹⁴. Below $\hbar\omega \approx 0.1$ meV ($\approx 1.6\times$ the instrumental resolution) the errors in S_{mag} increase strongly (some data points fall even outside the plotted range), since the strong elastic scattering S_{ela} is subtracted from the total scattering to receive S_{mag} and due to small uncertainties in the resolution function. These uncertainties are the same for both data sets and do not play a role since only the difference is analysed for the estimation of the exchange energy saving. (b) Linewidth Γ vs. temperature T of the quasielastic magnetic response at Q_{AF} in the normal state as yielded by fits to the data shown in Fig. 2. Plotted here is $\Gamma(T) - \Gamma_0$ vs. T , with $\Gamma_0 = 0.112$ meV. The solid line $\Gamma(T) - \Gamma_0 = aT^{3/2}$ (with $a = 0.061$ meV/K^{1.5}) is the expected behaviour near a 3D SDW QCP. (c) Temperature dependence of the spin excitation gap $\hbar\omega_{gap}$ at Q_{AF} together with the scaled d-wave BCS superconducting gap function (solid line). The error bars denote the statistical error.

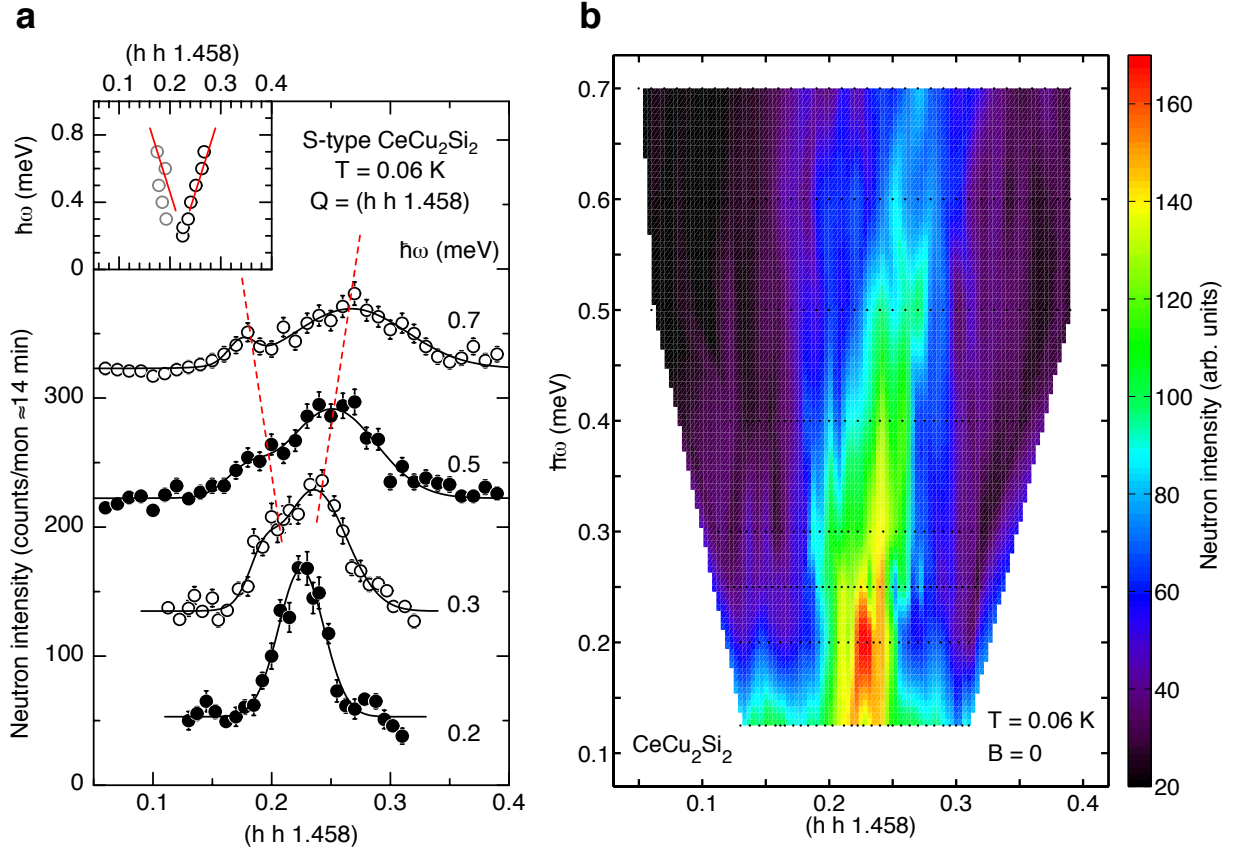


FIG. 4: **Dispersion of the magnetic response in superconducting CeCu_2Si_2 .** (a) Wave vector \mathbf{Q} dependence of the magnetic response around \mathbf{Q}_{AF} in S-type CeCu_2Si_2 in the superconducting state at $T = 0.06$ K for different energy transfers $\hbar\omega$. The scans are shifted by 100 counts with respect to each other. Solid lines denote fits of two peaks with Gaussian lineshape to the data, while dashed lines are only guides to the eye. From the linewidth at small energy transfers a dynamic correlation length $\xi \approx 25$ Å is inferred. Inset: Dispersion of the magnetic excitation around \mathbf{Q}_{AF} at $T = 0.06$ K as a result of the fits to the \mathbf{Q} scans. The solid line indicates a fit to the data with a linear dispersion relation yielding a velocity $v_{\text{exc}} = (4.44 \pm 0.86) \text{ meV}\text{\AA}$ (for comparison spin-wave velocities in other HF metals, UPd_2Al_3 : $v = 10 - 15 \text{ meV}\text{\AA}$ ³⁷, URu_2Si_2 : $v \approx 45 \text{ meV}\text{\AA}$ ⁴³). The error bars represent the statistical error. (b) Colour coded intensity plot of the data displayed in (a) and additional data, clearly indicating the dispersion of the gapped spin excitation. Black dots mark the (\mathbf{Q}, ω) positions data were taken.

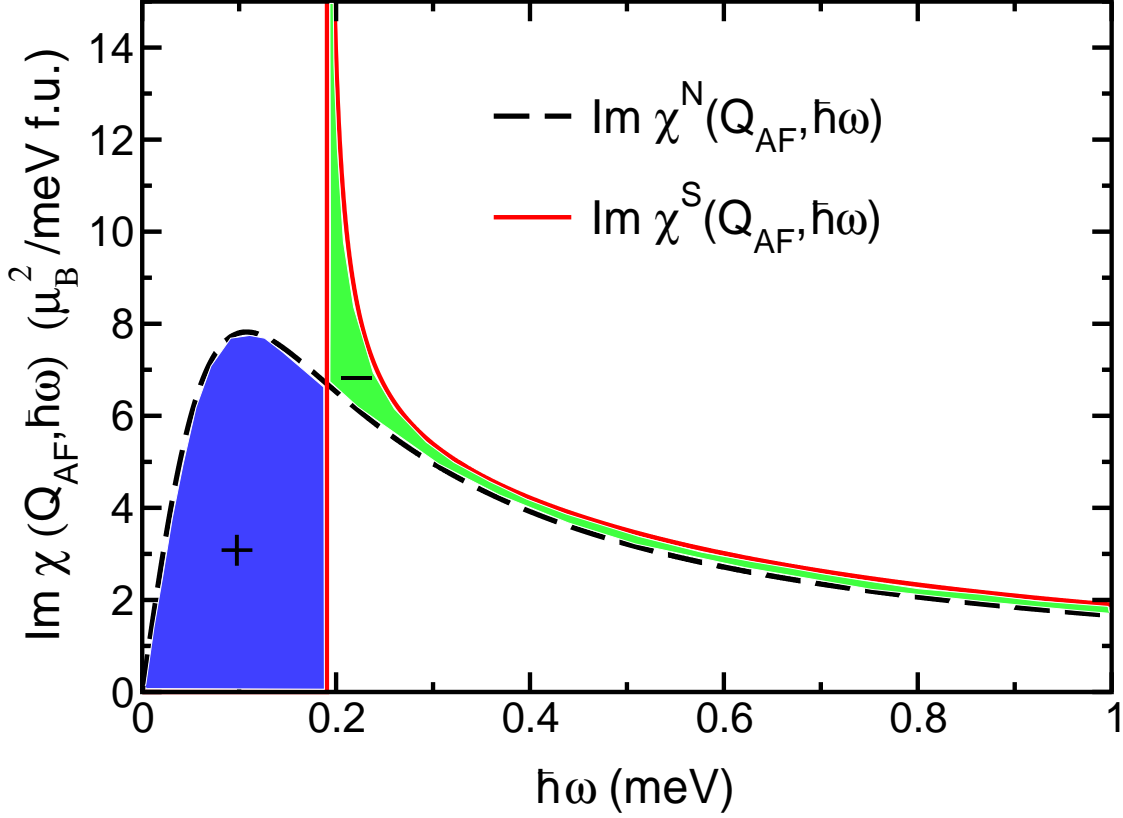


FIG. 5: Schematic plot of the imaginary part of the dynamic spin susceptibility $\text{Im}\chi(\mathbf{Q}_{\text{AF}}, \omega)$ in the normal (N) and superconducting (S) states. The dynamic correlation function $S(\mathbf{Q}_{\text{AF}}, \omega)$ of Figure 3(a) is related to $\text{Im}\chi(\mathbf{Q}_{\text{AF}}, \omega)$ via the fluctuation-dissipation theorem after de-convolving the data with the instrument's energy resolution function. The blue area marked with a '+' contributes to an increase in ΔE_x whereas the green area (marked with a '-') leads to a decrease in ΔE_x . The fact that the opening of the gap contributes to the saving in exchange energy is a consequence of $I(\mathbf{Q}_{\text{AF}}) > 0$ at the wave vector \mathbf{Q}_{AF} , where $\text{Im}\chi^{N/S}(\mathbf{Q}, \omega)$ is peaked.

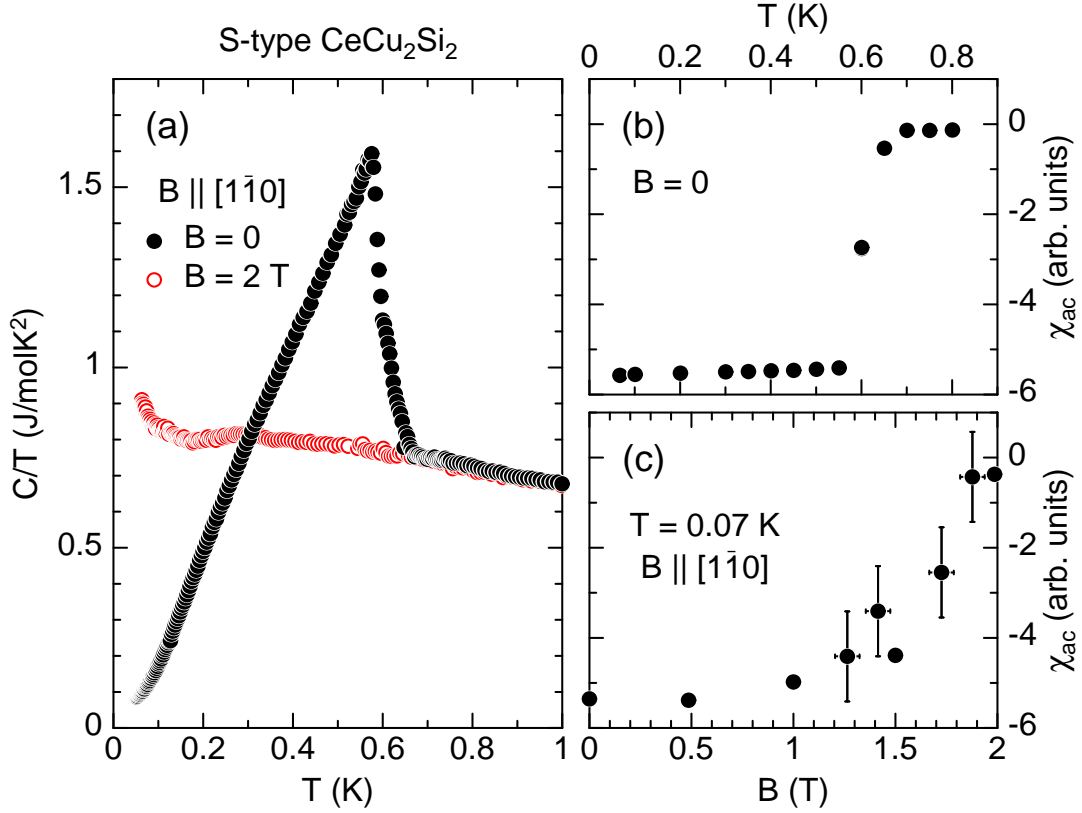


FIG. 6: (a) Specific heat C of the same S-type CeCu_2Si_2 single crystal which was studied by neutron scattering, plotted as C/T versus temperature T in zero magnetic field $B = 0$ and a magnetic field $B = 2$ T applied along $[1\bar{1}0]$. (b) Temperature dependence of the ac susceptibility χ_{ac} at $B = 0$. (c) Magnetic field dependence of χ_{ac} at a temperature $T = 0.07$ K and in a magnetic field $B \parallel [1\bar{1}0]$. The data with large error bars were taken when sweeping the magnetic field while all other data were measured during neutron scattering scans where the magnetic field was constant for a long time.

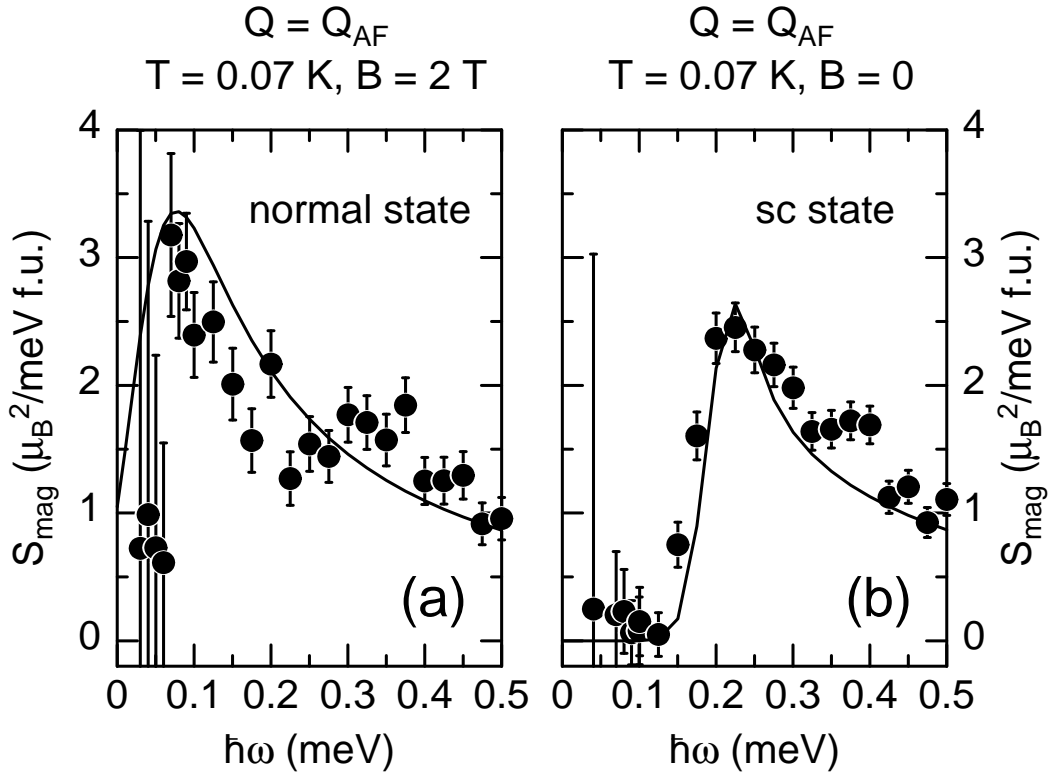


FIG. 7: Magnetic response at Q_{AF} in (a) the normal and (b) the superconducting states of CeCu_2Si_2 (same data as in Fig. 3(a)). Solid lines are fits to the data (see text). For energies $\hbar\omega > 0.5 \text{ meV}$, the dynamical susceptibility of the normal and superconducting states coincide (within the experimental error bars) and thus do not contribute to the exchange energy saving.